Li–O_2 Batteries

Deutsche Ausgabe: DOI: 10.1002/ange.201605228
Internationale Ausgabe: DOI: 10.1002/anie.201605228

Amorphous Li_2O_2: Chemical Synthesis and Electrochemical Properties

*Yelong Zhang, Qinghua Cui, Xinmin Zhang, William C. McKee, Ye Xu, Shigang Ling, Hong Li, Guiming Zhong, Yong Yang, and Zhangquan Peng**

Abstract: *When aprotic Li–O_2 batteries discharge, the product phase formed in the cathode often contains two different morphologies, that is, crystalline and amorphous Li_2O_2. The morphology of Li_2O_2 impacts strongly on the electrochemical performance of Li–O_2 cells in terms of energy efficiency and rate capability. Crystalline Li_2O_2 is readily available and its properties have been studied in depth for Li–O_2 batteries. However, little is known about the amorphous Li_2O_2 because of its rarity in high purity. Herein, amorphous Li_2O_2 has been synthesized by a rapid reaction of tetramethylammonium superoxide and $LiClO_4$ in solution, and its amorphous nature has been confirmed by a range of techniques. Compared with its crystalline siblings, amorphous Li_2O_2 demonstrates enhanced charge-transport properties and increased electro-oxidation kinetics, manifesting itself a desirable discharge phase for high-performance Li–O_2 batteries.*

By replacing the conventional lithium-based intercalation chemistry with highly exergonic conversion reactions, a step-change in energy density can be achieved for the resultant energy-storage devices, among which the aprotic Li–O_2 battery has attracted much attention.[1,2] Operation of the aprotic Li–O_2 battery relies on the O_2 reduction reaction forming solid Li_2O_2 in the positive electrode on discharge, and the reverse Li_2O_2 oxidation releasing O_2 upon recharge.[3–5] Depending on the Li–O_2 cell's operating conditions (discharging rate and overpotential)[6–8] and configurations (cathode material, electrolyte, and catalyst),[9–13] two distinct morphologies of the product phase have been frequently identified at the end of discharge, which include crystalline (typically toroid-shaped) and amorphous (typically film-like) Li_2O_2.[14] The morphology of Li_2O_2 has been recognized to impact strongly on the electrochemical performance (particularly charging) of Li–O_2 cells in terms of energy efficiency and rate capability, see recent works by Adams et al.[7] and Lu et al.[13] As a result, considerable research efforts have been devoted to the understanding of the formation and growth, charge transport, and defect chemistry of Li_2O_2 in the past few years.[3–14]

So far, it is generally accepted that crystalline Li_2O_2, which is detectable by powder X-ray diffraction (PXRD), can be electro-deposited at low current densities or overpotentials, and usually has a toroid-shaped appearance with dimensions of hundreds of nanometers.[5] The formation of large Li_2O_2 particles suggests that unconventional charge-transport pathways or diffusion of soluble intermediates may operate in the discharge process. For example, charge transport via surface,[15] grain boundaries,[16] or defects[17] in bulk of crystalline Li_2O_2 have been proposed for the growth of large particulate Li_2O_2. In addition, dissolution of O_2^- and LiO_2 promoted by additives (e.g. H_2O)[18] or high-donor-number electrolyte solvents[9] have been suggested to drive solution-mediated Li_2O_2 formation, which is not limited by the transport properties of Li_2O_2. Meanwhile, solid-state studies on nominally pure, crystalline Li_2O_2 (i.e., chemical Li_2O_2)[19,20] found that the electronic conductivity of crystalline Li_2O_2 is very limited and cannot support electrons traveling long distances to reach the reaction sites that have been presumed to be at the $Li_2O_2|Li^+$ electrolyte interface.[21–23] Therefore, a solution-mediated pathway is more likely for the formation of large Li_2O_2.[8,24,25] Because of its poor conductivities, crystalline Li_2O_2 has been found to be difficult to decompose and usually a large overpotential ($\eta > 1$ V) is required for the charging of Li–O_2 cells containing electro-deposited crystalline Li_2O_2[26] or commercial Li_2O_2.[27,28]

Although the discharge product of aprotic Li–O_2 batteries was at one time presumed to be crystalline Li_2O_2, mounting evidence has suggested the presence of amorphous Li_2O_2, which can be promoted by higher discharging rates,[7,12] larger overpotentials,[7] and certain electro-catalysts.[10,11,13] Amorphous Li_2O_2 has been theoretically studied by Tian et al. using first-principles "melt-and-quench" molecular dynamics coupled with percolation theory, and enhanced charge transport properties, compared with crystalline Li_2O_2, have been predicted.[24] Until now, experimental studies on amorphous Li_2O_2 are limited to Li–O_2 cathodes electrochemically discharged at higher rates (presumably forming amorphous Li_2O_2), which, however, could be complicated by the side reaction products during discharge[29] and by the adventitiously co-formed crystalline Li_2O_2.[12] Moreover, the intrinsic

[*] Y. Zhang, Dr. Q. Cui, Dr. X. Zhang, Prof. Z. Peng
State Key Laboratory of Electroanalytical Chemistry
Changchun Institute of Applied Chemistry
Chinese Academy of Science
Changchun, Jilin, 130022 (China)
E-mail: zqpeng@ciac.ac.cn
Y. Zhang
University of Chinese Academy of Science
Beijing 100049 (China)
Dr. W. C. McKee, Prof. Y. Xu
Department of Chemical Engineering, Louisiana State University
Baton Rouge, LA 70803 (USA)
S. Ling, Prof. H. Li
Institute of Physics, Chinese Academy of Sciences
Beijing, 100190 (China)
Dr. G. Zhong, Prof. Y. Yang
State Key Lab of Physical Chemistry of Solid Surfaces and College of Chemistry & Chemical Engineering, Xiamen University
Xiamen, 361005 (China)
Supporting information and the ORCID identification number(s) for the author(s) of this article can be found under http://dx.doi.org/10.1002/anie.201605228.

properties (e.g., charge transport and oxidation kinetics) of amorphous Li_2O_2 are largely unknown because of the unavailability of these compounds in high purity.

Herein, we report the chemical synthesis and electrochemical properties of amorphous Li_2O_2. The amorphous Li_2O_2 was prepared by a rapid disproportionation reaction of tetramethylammonium superoxide ($TMAO_2$) and $LiClO_4$ in acetonitrile, and its amorphous nature has been confirmed by a range of complementary techniques including powder X-ray diffraction (PXRD), transmission electron microscopy (TEM) coupled with selected area electron diffraction (SAED), and Raman spectroscopy. Solid-state studies by conductivity measurement, nuclear magnetic resonance (NMR), and electron spin resonance (ESR) techniques, together with electrochemical studies by differential electrochemical mass spectrometry (DEMS), indicated that amorphous Li_2O_2, compared with its crystalline siblings, possesses enhanced charge-transport properties (higher ionic and electronic conductivities) and increased oxidation kinetics (lower oxidation overpotentials). Combined, these results suggest that amorphous Li_2O_2 is a desirable discharge phase for high-performance aprotic Li–O_2 batteries, and that pursuing the combinations of cathode material, electrolyte, and catalyst that can promote the formation of amorphous Li_2O_2 at a broad range of discharging rates will contribute greatly to the future development of aprotic Li–O_2 batteries.

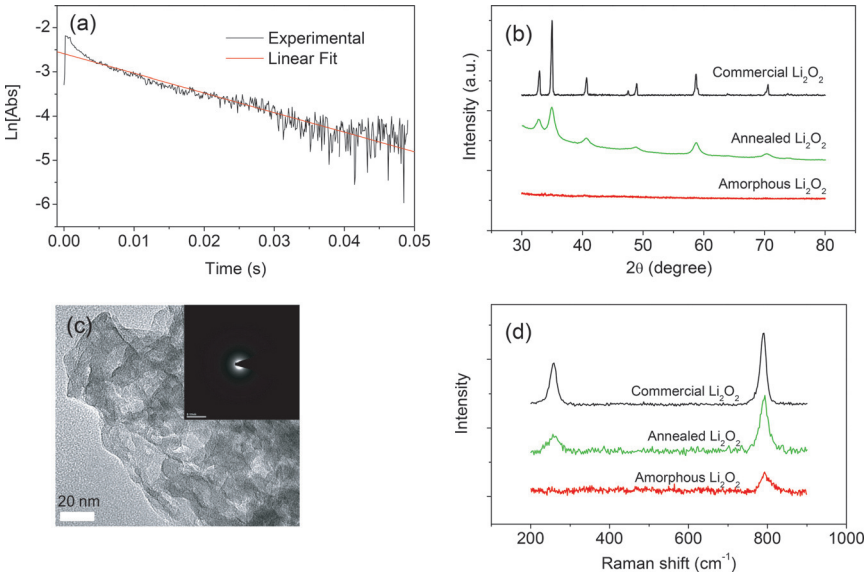

Figure 1. a) Reaction of 1 mM $TMA^+O_2^-$ and 100 mM $LiClO_4$ in acetonitrile studied with stopped-flow UV/Vis spectrophotometry, b) PXRD patterns of synthesized, annealed, and commercial Li_2O_2, c) TEM image and SAED (inset) of synthesized Li_2O_2, and d) Raman spectra of the various Li_2O_2 compounds.

Amorphous Li_2O_2 was synthesized by a disproportionation reaction of $TMAO_2$ (1.102 g) and $LiClO_4$ (1.404 g) in acetonitrile at room temperature. $TMAO_2$ was used as a precursor because of its excellent solubility in common organic solvents.[30] The detailed synthesis and characterization of $TMAO_2$ can be found in Ref. [8]. The reaction of $TMAO_2$ and $LiClO_4$ producing solid Li_2O_2 and gaseous O_2 has been quantitatively studied in dimethyl sulfoxide (DMSO) before, in which a rate constant of $k_2 = 24.6\,M^{-1}s^{-1}$ was measured and nano-crystalline Li_2O_2 with an average size of about 9 nm was obtained.[8]

In this work, we use acetonitrile as the reaction medium because of its lower solvating ability (donor number 14 vs. 30 of DMSO), which could essentially increase the reaction kinetics because of the less buffered reactivity (more exactly, acidity) of Li^+ ions toward O_2^-, favoring the formation of Li_2O_2 with even smaller size or amorphous phase.[31,32] The rate constant of the reaction of $TMAO_2$ and $LiClO_4$ in acetonitrile has been quantified to be $560\,M^{-1}s^{-1}$ by a stopped-flow UV/Vis spectrophotometer, which is more than 20 times faster than in DMSO, see Figure 1 a.

The reaction product, after washing copiously with acetonitrile and drying overnight under vacuum at room temperature, was subjected to the examination by PXRD, TEM coupled with SAED, and Raman spectroscopy (Figure 1 b–d). PXRD analysis showed a diffraction pattern that was essentially featureless (Figure 1 b red curve). However, annealing the product at 120 °C overnight led to the appearance of a set of diffraction peaks that can be indexed to the crystalline Li_2O_2 (Figure 1 b green curve). For comparison, PXRD result of the freshly ball-milled commercial Li_2O_2 was also included (Figure 1 b black curve).

Another evidence for the amorphous nature of the Li_2O_2 was from a TEM study coupled with SAED, in which a porous structure was observed (Figure 1 c) and no electron diffraction pattern of any periodic structures was observed (Figure 1 c, inset), while more compact structures (Figure S1 and S2 in the Supporting Information) and well-defined electron diffraction patterns (rings and spots in the insets of Figure S1 and S2) were obtained for the annealed and commercial Li_2O_2, suggesting the improvement in the crystallinity upon annealing at elevated temperatures. In addition, a scanning electron microscopy (SEM) study provided the complementary morphological information of the three Li_2O_2 samples including their particle size, agglomeration extent, and surface area (amorphous > annealed > commercial), see Figure S3.

A Raman spectroscopic study of the as-prepared, annealed and commercial Li_2O_2 (Figure 1 d) demonstrated that they were all peroxides having a Raman band of around 788 cm^{-1} assigned to the stretching vibration of LiO–OLi. However, the much decreased Raman signal intensity, broadened full wave at half maximum (FWHM, ca. 36 cm^{-1} vs. 16 cm^{-1} of commercial Li_2O_2) of LiO–OLi stretching, and particularly the absence of the Li–O lattice vibration (258 cm^{-1}) for the as-prepared Li_2O_2 indicated that the synthesized Li_2O_2 was amorphous (Figure 1 d red curve). The recovery of Li–O vibration by annealing at 120 °C

(Figure 1 d green curve) also suggested the improvement in the crystallinity. Similar Raman spectroscopic features have been observed for the lattice vibrations (M–O) of other metal oxides with amorphous structures (or poor crystallinity), such as TiO_2,[33] ZrO_2,[34] CuO,[35] and Fe_2O_3.[36] We did not exclude the possibility that the grain size of the synthesized Li_2O_2 was so small that it could not be detected by PXRD and SAED, with the SAED having the ability to decompose its structure.[37]

After confirming the amorphous nature of the synthesized Li_2O_2, electrochemical studies have been conducted to get the fundamental information of its charge-transport properties and oxidation kinetics. Transport properties were investigated by a combination of AC impedance and DC polarization techniques at room temperature, according to a procedure reported by Gerbig et al.,[19] see also Experimental Section in the Supporting Information for details of the pellet preparation and data analysis. The ionic (σ_{ion}) and electronic (σ_{eon}) conductivities of the amorphous Li_2O_2 were measured to be 7.10×10^{-8} S cm^{-1} and 5.02×10^{-9} S cm^{-1}, respectively (see Figure 2 a,b and Table S1), which are 2–3 orders of magnitude higher than those of nano-Li_2O_2 at room temperature by Dunst et al.[20] For comparison, conductivity measurements have also been conducted on annealed and commercial Li_2O_2, and much smaller values were obtained, see Figure 2 c–f and Table S1.

It has been independently identified by Gerbig et al.[19] and Radin and Siegel[17] that the ionic conductivity of Li_2O_2 is via lithium vacancies and the electronic conductivity via electron holes, that is, localized O_2^- ions. To understand the enhanced σ_{ion} and σ_{eon} of amorphous Li_2O_2, solid state studies using NMR spectroscopy (Figure S4 and Table S2) to probe the Li^+ mobility and ESR spectroscopy (Figure S5) to probe the density of localized O_2^-, respectively, have been conducted. NMR spectroscopic results indicated that the dominating spin-lattice relax time (T_1), for example at 298 K, was in the following order of amorphous Li_2O_2 (1.17 s) < annealed Li_2O_2 (6.87 s) < commercial Li_2O_2 (122 s), in which a smaller T_1 suggests a higher Li^+ mobility. More T_1 values at various temperatures are compiled in Table S2, and were qualitatively consistent with the ionic conductivity measurements (Table S1). The ESR study of the various Li_2O_2 compounds at 77 K indicated that the amorphous Li_2O_2 has the highest density (40.8 ppm) of O_2^- defects (Figure S5), accounting for its relatively high electronic conductivity. However, annealing amorphous Li_2O_2 at 120 °C greatly annihilated the O_2^- defects (13.6 ppm) resulting in decreased electronic conductivity (Figure 2 c,d, and Table S1).

To shed light on the effects of the morphologies and conductivities on the oxidation kinetics of various Li_2O_2, a DEMS study has been conducted, where galvanostatic charging voltage profile and gaseous O_2 (and CO_2) evolution rate were recorded, simultaneously. For the preparation of the cathodes in discharged state, Li_2O_2, PVDF binder and Super P carbon (1:1:8 m/m) were dispersed in acetonitrile and applied to a carbon fiber paper current collector. The total mass loading of the cathode was about 30 mg. For the charging of the cathodes, a constant current of 0.2 mA (ca. 8 mA g$^{-1}_{carbon}$) was applied, and to avoid excess parasitic reactions during charging only about 10% of the total capacity of the cathodes was charged.

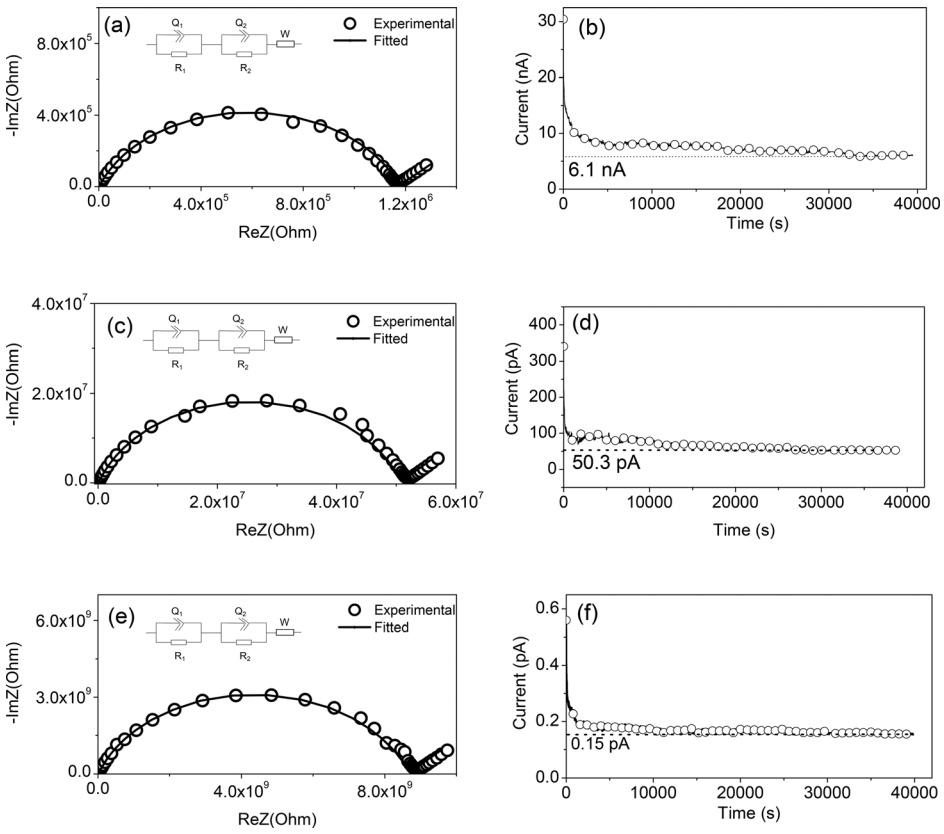

Figure 2. AC impedance (left) and DC polarization (right) measurements of a,b) amorphous, c,d) annealed, and e,f) commercial Li_2O_2. Insets in (a,c,e) show the equivalent circuits used to fit the impedance spectra.

Figure 3 a–c show the DEMS results, in which an average charging plateau of 3.54 V versus Li/Li$^+$ was obtained for the oxidation of amorphous Li_2O_2, while plateaus of 3.82 and 4.04 V were observed for the annealed and commercial Li_2O_2, respectively. Extended Li_2O_2 oxidation (i.e., > 10% of the packed capacity) showed that O_2 evolution was accompanied by CO_2 release at the late stage of charging, indicating the decomposition of cathode materials and electrolytes at high voltages,[28] see Fig-

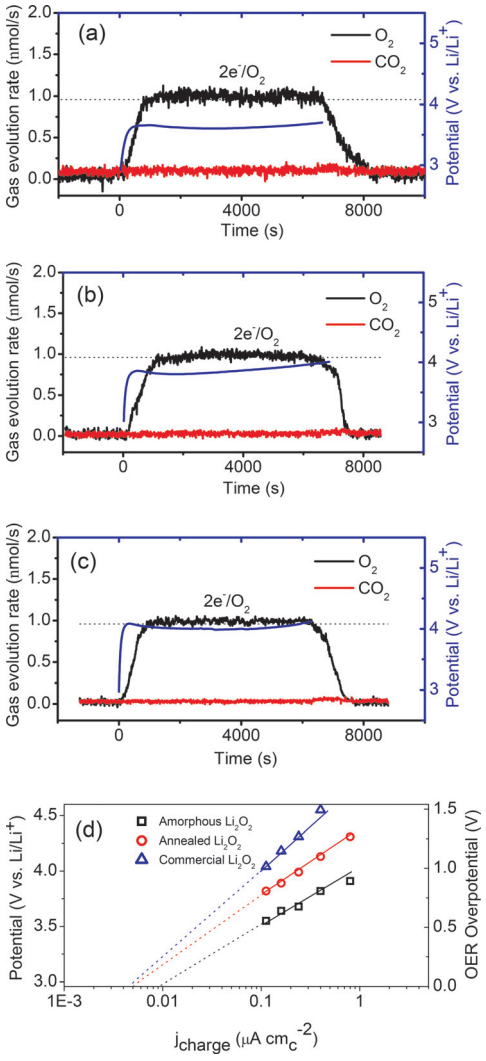

Figure 3. DEMS results of charging a Li–O_2 cathode containing a) amorphous, b) annealed, and c) commercial Li_2O_2 with a constant current of 0.2 mA (ca. 8 mA g^{-1}_{carbon}). d) Tafel plot of galvanostatic charging voltage versus carbon true surface area normalized current for electrodes containing various Li_2O_2.

ure S6. The DEMS results provide compelling evidence that the amorphous Li_2O_2 having higher σ_{ion} and σ_{eon} can indeed be decomposed with lower overpotentials (i.e., higher oxidation kinetics). More kinetics information of the amorphous Li_2O_2 oxidation has been obtained by charging the cathodes with various current densities (Figure S7) and thereafter constructing a Tafel plot (Figure 3d). An exchange current density of 9.5 nA cm^{-2} (normalized to the true surface area of the Super P carbon) has been observed for amorphous Li_2O_2, while lower values were obtained for annealed (5.2 nA cm^{-2}) and commercial (4.0 nA cm^{-2}) Li_2O_2. Although the exchange currents are normalized to the true surface area of the composite carbon electrodes, the oxidation kinetics would also be sensitive to the surface area of Li_2O_2, particularly for the amorphous one having highest surface area.

In summary, amorphous Li_2O_2 has been synthesized by a rapid reaction of $TMAO_2$ and $LiClO_4$ in acetonitrile, and its amorphous nature has been confirmed by a range of complementary techniques. Conductivity measurements indicated that the amorphous Li_2O_2, compared with its crystalline siblings, possesses improved charge-transport properties rising from the enhanced Li^+ mobility and increased O_2^- concentration within the amorphous Li_2O_2, results which are supported by solid-state studies using NMR and ESR spectroscopy techniques. In addition, a DEMS study provided direct evidence that amorphous Li_2O_2 can be decomposed at a much lower potential than crystalline Li_2O_2 under the same charging current density. These results suggest that amorphous Li_2O_2 is a desirable discharge phase for high-performance aprotic Li–O_2 batteries, and that pursuing the combinations of cathode material, electrolyte, and catalyst that can promote the formation of amorphous Li_2O_2 at a broad range of discharging rates will contribute greatly to the future development of Li–O_2 batteries.

Acknowledgements

Z.P. is indebted to the National Natural Science Foundation of China (Grant No. 21575135 and 91545129), the "Strategic Priority Research Program" of the CAS (Grant No. XDA09010401), the Ministry of Science and Technology of China (Grant No. 2016YBF0100100), the "Recruitment Program of Global Youth Experts" of China, the Science and Technology Development Program of the Jilin Province (Grant No. 20150623002TC and 20160414034GH) and the Natural Science Foundation of Jiangsu Province (Grant No. BK20131139).

Keywords: amorphous Li_2O_2 · aprotic Li–O_2 batteries · charge-transport properties · oxidation kinetics

How to cite: *Angew. Chem. Int. Ed.* **2016**, *55*, 10717–10721
Angew. Chem. **2016**, *128*, 10875–10879

[1] M. Armand, J. M. Tarascon, *Nature* **2008**, *451*, 652–657.
[2] P. G. Bruce, S. A. Freunberger, L. J. Hardwick, J. M. Tarascon, *Nat. Mater.* **2012**, *11*, 19–29.
[3] J. Lu, L. Li, J.-B. Park, Y.-K. Sun, F. Wu, K. Amine, *Chem. Rev.* **2014**, *114*, 5611–5640.
[4] A. C. Luntz, B. D. McCloskey, *Chem. Rev.* **2014**, *114*, 11721–11750.
[5] N. Imanishi, A. C. Luntz, P. G. Bruce, *The Lithium Air Battery*: *Fundamentals*, Springer, New York, **2014**.
[6] Y. C. Lu, D. G. Kwabi, K. P. Yao, J. R. Harding, J. Zhou, L. Zuin, Y. Shao-Horn, *Energy Environ. Sci.* **2011**, *4*, 2999–3007.
[7] B. D. Adams, C. Radtke, R. Black, M. L. Trudeau, K. Zaghib, L. F. Nazar, *Energy Environ. Sci.* **2013**, *6*, 1772–1778.
[8] Y. Zhang, X. Zhang, J. Wang, W. C. McKee, Y. Xu, Z. Peng, *J. Phys. Chem. C* **2016**, *120*, 3690–3698.
[9] L. Johnson, C. Li, Z. Liu, Y. Chen, S. A. Freunberger, P. C. Ashok, B. B. Praveen, K. Dholakia, J.-M. Tarascon, P. G. Bruce, *Nat. Chem.* **2014**, *6*, 1091–1099.
[10] H. G. Jung, Y. S. Jeong, J. B. Park, Y. K. Sun, B. Scrosati, Y. J. Lee, *ACS Nano* **2013**, *7*, 3532–3539.
[11] E. Yilmaz, C. Yogi, K. Yamanaka, T. Ohta, H. R. Byon, *Nano Lett.* **2013**, *13*, 4679–4684.
[12] H. G. Jung, H. S. Kim, J. B. Park, I. H. Oh, J. Hassoun, C. S. Yoon, Y. K. Sun, *Nano Lett.* **2012**, *12*, 4333–4335.

[13] J. Lu, Y. Lei, K. C. Lau, X. Luo, P. Du, J. Wen, R. S. Assary, U. Das, D. J. Miller, J. W. Elam, H. M. Albishri, D. A. El-Hady, Y.-K. Sun, L. A. Curtiss, K. Amine, *Nat. Commun.* **2013**, *4*, 2383.
[14] P. Adelhelm, P. Hartmann, C. L. Bender, M. Busche, C. Eufinger, J. Janek, *Beilstein J. Nanotechnol.* **2015**, *6*, 1016 – 1055.
[15] M. D. Radin, J. F. Rodriguez, F. Tian, D. J. Siegel, *J. Am. Chem. Soc.* **2012**, *134*, 1093 – 1103.
[16] W. T. Geng, B. L. He, T. Ohno, *J. Phys. Chem. C* **2013**, *117*, 25222 – 25228.
[17] M. D. Radin, D. J. Siegel, *Energy Environ. Sci.* **2013**, *6*, 2370 – 2379.
[18] N. B. Aetukuri, B. D. McCloskey, J. M. García, L. E. Krupp, V. Viswanathan, A. C. Luntz, *Nat. Chem.* **2015**, *7*, 50 – 56.
[19] O. Gerbig, R. Merkle, J. Maier, *Adv. Mater.* **2013**, *25*, 3129 – 3133.
[20] A. Dunst, V. Epp, I. Hanzu, S. A. Freunberger, M. Wilkening, *Energy Environ. Sci.* **2014**, *7*, 2739 – 2752.
[21] V. Viswanathan, K. S. Thygesen, J. S. Hummelshøj, J. K. Nørskov, G. Girishkumar, B. D. McCloskey, A. C. Luntz, *J. Chem. Phys.* **2011**, *135*, 214704.
[22] M. D. Radin, C. M. Monroe, D. J. Siegel, *J. Phys. Chem. Lett.* **2015**, *6*, 3017 – 3022.
[23] K. B. Knudsen, A. C. Luntz, S. H. Jensen, T. Vegge, *J. Phys. Chem. C* **2015**, *119*, 28292 – 28299.
[24] F. Tian, M. D. Radin, D. J. Siegel, *Chem. Mater.* **2014**, *26*, 2952 – 2959.
[25] D. G. Kwabi, M. Tułodziecki, N. Pour, D. M. Itkis, C. V. Thompson, Y. Shao-Horn, *J. Phys. Chem. Lett.* **2016**, *7*, 1204 – 1212.
[26] B. M. Gallant, D. G. Kwabi, R. R. Mitchell, J. Zhou, C. V. Thompson, Y. Shao-Horn, *Energy Environ. Sci.* **2013**, *6*, 2518 – 2528.
[27] T. Ogasawara, A. Debart, M. Holzapfel, P. Novak, P. G. Bruce, *J. Am. Chem. Soc.* **2006**, *128*, 1390 – 1393.
[28] S. Meini, N. Tsiouvaras, K. U. Schwenke, M. Piana, H. Beyer, L. Lange, H. A. Gasteiger, *Phys. Chem. Chem. Phys.* **2013**, *15*, 11478 – 11493.
[29] S. A. Freunberger, Y. Chen, N. E. Drewett, L. J. Hardwick, F. Bard, P. G. Bruce, *Angew. Chem. Int. Ed.* **2011**, *50*, 8609 – 8613; *Angew. Chem.* **2011**, *123*, 8768 – 8772.
[30] P. D. C. Dietzel, K. Kremer, M. Jansen, *J. Am. Chem. Soc.* **2004**, *126*, 4689 – 4696.
[31] J. W. Morse, W. H. Casey, *Am. J. Sci.* **1988**, *288*, 537 – 560.
[32] T. P. Feenstra, P. L. De Bruyn, *J. Colloid Interface Sci.* **1981**, *84*, 66 – 72.
[33] K. Liang, B. K. Tay, O. V. Kupreeva, T. I. Orekhovskaya, S. K. Lazarouk, V. E. Borisenko, *ACS Sustainable Chem. Eng.* **2014**, *2*, 991 – 995.
[34] F. Liu, J. Yang, T. Zhao, *Phys. Rev. B* **1997**, *55*, 8847.
[35] J. F. Xu, W. Ji, Z. X. Shen, W. S. Li, S. H. Tang, X. R. Ye, D. Z. Jia, X. Q. Xin, *J. Raman Spectrosc.* **1999**, *30*, 413 – 415.
[36] W. Chen, X. Pan, X. Bao, *J. Am. Chem. Soc.* **2007**, *129*, 7421 – 7426.
[37] H. Zheng, D. D. Xiao, X. Li, Y. Liu, Y. Wu, J. Wang, K. Jiang, C. Chen, L. Gu, X. Wei, Y. Hu, Q. Chen, H. Li, *Nano Lett.* **2014**, *14*, 4245 – 4249.

Received: May 29, 2016
Revised: June 27, 2016
Published online: August 3, 2016

